Solar Cycle Variation of Outer Belt Electron Dose at Low-Earth Orbit

D. H. Brautigam, B. K. Dichter, Kevin P. Ray, W. Rhett Turnbull, D. Madden, A. Ling, E. Holeman, Robert H. Redus, and S. Woolf

***Abstract*—The solar cycle dependence of dose rates in the low-altitude "horns" of the outer zone electron belt is examined using data from TSX5/CEASE (solar maximum epoch) and APEX/PASP+ (solar minimum epoch). It is found, after normalizing the dose rates to account for the different shielding geometries, that the ratio of PASP to CEASE dose rates is $\sim$4 for $L > 4$. This is contrary to the equal dose rates predicted by the NASA AE8MIN and AE8MAX models.**

***Index Terms*—Electron dose, low earth orbit, radiation belt, solar cycle variation.**

I. Introduction

THE U.S. Air Force Compact Environmental Anomaly Sensor (CEASE) [1] was launched into low-earth orbit on the Tri-Service Experiment-5 (TSX5) on June 7, 2000, and began returning data the following day. The experiment was integrated and flown by the Department of Defense Space Test Program and is expected to operate through October 2001. Its 13 months of operation to date have spanned a period of solar maximum peak activity. The TSX5 low-earth orbit is similar to that of the APEX spacecraft on which the PASP+ dosimeter [2], [3] operated during the two years (1994 to 1996) leading up to solar minimum. These two data sets provide the opportunity to study the solar cycle dependence of the outer radiation belt electron dose.

It is well known that the highly variable outer radiation belt megaelectronvolt electron population contributes to spacecraft system degradation through deep dielectric charging and radiation dose [4], [5]. This particle population also represents a radiation hazard to astronauts, particularly if extravehicular activities are scheduled during magnetically disturbed conditions when the outer radiation belt is inflated with intense fluxes [6]. Thus, there is a great incentive to improve understanding of the dynamics of this particle population and develop more accurate models with which to specify this environment.

Geosynchronous spacecraft provide the necessary long-term continuous database for studying solar cycle variations of the outermost boundary of the outer belt. Such studies have found that during the two to three years preceding solar minimum, the megaelectronvolt electrons at geosynchronous altitude exhibit episodic enhancements with a 27-day periodicity attributed to the well-structured high-speed solar wind streams (HSSWSs) that flow from coronal holes near the solar ecliptic plane during this phase of the solar cycle [7]–[9]. This periodic behavior has also been observed in dose measurements at low-altitude polar orbit [10]–[12]. This presolar minimum enhanced activity results in yearly averaged geosynchronous fluxes of $>$3 MeV electrons, which can be $\sim$8 times higher than the corresponding averages around solar maximum [9].

The trapped electron environment has been characterized by long-term average models (NASA solar minimum AE8MIN and maximum AE8MAX [13]) and magnetic activity-dependent models (APEXRAD [3], CRRESRAD [14], and CRRESELE [15]). The solar cycle phase dependence of geosynchronous electrons referred to earlier is inconsistent with the NASA AE8 electron models, which show that the geosynchronous ($L = 6.6$) integral flux of $>$3 MeV electrons during solar maximum and solar minimum are equivalent [13]. Other deficiencies of currently available models have been discussed previously [16], [17]. Spacecraft design engineers are interested not just in long-term average radiation belt models (either current or some future improved version) but also in models that give the probability of encountering various levels of radiation as a function of solar cycle phase.

This study examines the solar cycle dependence of dose in the low-altitude high-latitude "horns" of the outer zone electron belt. Both mission-average dose and probability distribution models are created for the APEX and TSX5 epochs that encompass solar minimum and maximum, respectively. These models show that for the epochs studied, the outer zone average dose rate from electrons is a factor of $\sim$4 higher (for $L > 4$) and peak at higher L during solar minimum than during solar maximum. Section II describes the relevant details of the spacecraft orbits and dosimeters, and Section III discusses the construction of the models. Section IV discusses the results, and Section V concludes with a summary.

II. Satellite Orbits and Dosimeters

The APEX satellite was launched on August 5, 1994, into a 70° inclination orbit with a perigee of 362 km, an apogee of 2544 km, and an orbital period of 115 min. The mission had some downtime, but remained active through May 1996 (solar minimum), with the PASP+ dosimeter returning approximately 12 months of data. The TSX5 satellite was launched on June

Manuscript received July 17, 2001. This work was supported by AFRL under Contracts F19628-00-C-0073 (Boston College), F19628-96-C-0063 (Amptek), F19628-00-C-0089 (Radex), and F19628-99-C-0077 (Arcon).

D. H. Brautigam, B. K. Dichter, K. P. Ray, and W. R. Turnbull are with the Air Force Research Laboratory, Space Vehicles Directorate, Hanscom AFB, MA 01731 USA (e-mail: Donald.Brautigam@hanscom.af.mil).

D. Madden and E. Holeman are with the Institute for Scientific Research, Boston College, Boston, MA 02467 USA.

A. Ling is with Radex, Inc., Bedford, MA 01730 USA.

R.H. Redus is with Amptek, Inc., Bedford, MA 01730 USA.

S. Woolf is with Arcon Corporation, Waltham, MA 02451 USA

Publisher Item Identifier S 0018-9499(01)10683-0.

7, 2000, into a 69° inclination orbit with a perigee of 410 km, an apogee of 1710 km, and an orbital period of 105 min. The CEASE dosimeter has been returning data continuously (with occasional minor data gaps) to date, resulting in more than 12 months of data for analysis. The solar cycle phases of the APEX and TSX5 satellite epochs are shown in Fig. 1. The APEX epoch spans the ∼2 y leading into solar minimum (May 1996), and the TSX5 epoch includes ∼1 y about solar maximum.

Both the PASP+ and CEASE dosimeters are constructed with an electrically active silicon diode sensor behind an aluminum (Al) shield of a prescribed thickness, which determines the threshold energy of particles that can penetrate the shield and deposit energy in the silicon sensor. The PASP+ dosimeter instrument includes four individual dosimeter heads (D1, D2, D3, D4) providing measurements from a range of particle energies [2], [3]. The D2 dosimeter head includes two different sized silicon diode sensors beneath an aluminum dome shield, D2B being the larger of the two. The CEASE instrument includes two dosimeter heads DD1 (thin shield) and DD2 (thick shield) [1]. Table I summarizes the main characteristics of the PASP+ D2B dosimeter and the CEASE DD1 dosimeter (which for simplicity will be referred to from here on as PASP and CEASE, respectively) that are relevant to this study. Although the Al shield thickness for the two dosimeters is comparable, the geometry is different; PASP is constructed with a hemispherical dome shield and CEASE with a planar shield. Particles following straight line paths toward the sensor from any point within the 2π field of view (FOV) outside the PASP dome will pass through equal pathlengths of Al shield. Although the planar dosimeter does not exhibit this spherical symmetry, it represents a more realistic geometry for simulating spacecraft shielding designs. The PASP and CEASE silicon diodes are of comparable thickness, yet the CEASE diode has a much greater planar dimension. The low linear energy transfer (LoLET) channel is defined by its energy deposition threshold settings (0.05–1.0 MeV for PASP and 0.05–0.85 MeV for CEASE). For ∼80 mil of Al shielding, electrons above ∼1 MeV and protons above 78 (for CEASE) to 115 MeV (for PASP) can penetrate the shielding and deposit the required energy for the LoLET channel. Although the >1 MeV electrons are the dominant source of LoLET dose in the outer radiation belt, the sporadic solar energetic proton events (most frequent during solar maximum) may contribute a relatively significant short-term LoLET dose over the course of a two- to three-day event. These events have been identified and are excluded from the database for this study.

Dose measurements are dependent on shielding characteristics (material, thickness, and geometry) and thus do not provide a direct measure of the environment as does a flux measurement, which discriminates particle species and energy. To substantiate any claim about the variable electron environment based on the comparison between two different dosimeter measurements on separate spacecraft, it is important to "normalize" their dose values to some reference. The relative response of the two dosimeters is investigated using the Integrated Tiger Series (ITS) electron transport code [18]. In this simulation, an isotropic power-law spectrum (1 to 10 MeV) is uniformly emitted from a virtual hemispherical surface centered on the

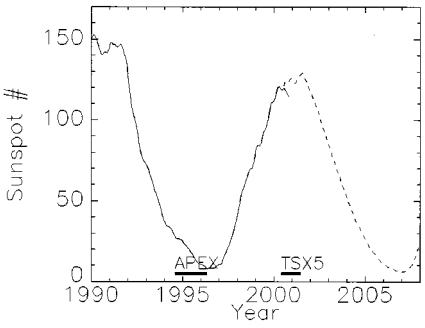

Fig. 1. The solar cycle is depicted here in terms of the smoothed sunspot number. The dashed curve beginning in mid-2001 is the predicted value. The mission time intervals for APEX (∼2 y leading into solar minimum) and TSX5 (∼1 y at solar maximum) are indicated by the heavy solid lines.

TABLE I
DOSIMETER CHARACTERISTICS

Dosimeter	Shield (Al)	Sensor (Si)		LoLET (MeV)	
Sensor head	Thick (mil) geometry	Area (cm^2)	Depth (cm)	Energy deposit	Electron threshold
PASP D2B	82.5 dome	0.051	0.038	0.05-1.0	≥ 1.0
CEASE DD1	80.0 planar	0.810	0.050	0.05-0.85	≥ 1.0

dosimeter sensor. Simulations are performed for a range of power-law indexes ($N = 2$ to 6) that are representative of the outer belt electron environment. The results show that for the hardest incident flux spectrum ($N = 2$), the dose ratio for the hemispheric to planar dosimeter is 2.0 and increases monotonically to 2.4 for the softest spectrum ($N = 6$), for an average ratio of 2.2. Because the planar dosimeter better represents spacecraft surface geometry, and because a number of CEASE units are planned for future flights, CEASE is taken as the reference standard here, and the PASP (hemispheric) dose is normalized to CEASE dose by dividing by a factor of 2.2.

Another issue to consider when comparing particle data from different instruments, even from the same spacecraft, is their FOV relative to the geomagnetic field. This determines the particle pitch angle distribution being sampled (the pitch angle is the angle between the particle velocity and the local geomagnetic field vectors). A collimated particle telescope pointing in a direction orthogonal to the geomagnetic field can see orders of magnitude higher particle fluxes (at 90° pitch angle) than an identical instrument pointing parallel (antiparallel) to the field line at 0° (180°) pitch angle. The APEX and TSX5 spacecraft are both three-axes stabilized. The APEX attitude control system maintained a solar inertial reference with PASP pointing nearly parallel (within 5°) to the ecliptic plane and orthogonal to the Earth–Sun line. The TSX5 attitude control system maintains a geocentric reference with CEASE pointing in a direction orthogonal to the spacecraft velocity vector and pointing 30° from the zenith direction. Assuming a collimated FOV direction normal to the dosimeter face (in actuality, each dosimeter has a full 2π steradian FOV), a pitch angle histogram was created, and a mission average computed for each dosimeter. With the 0° to 180° pitch angle distribution collapsed to a 0° to 90° distribution, the average values were

found to be 35° (CEASE) and 50° (PASP) over the range from $L = 3$ to 6.5. This marginal difference in average pitch angle represents a negligible effect, particularly given the fact that the two dosimeters are not collimated but have a full 2π steradian FOV. The difference in PASP and CEASE orientation is thus assumed to be an insignificant factor in comparing the daily average dose rates.

III. Analysis

Since radiation belt particle motion is tied to the geomagnetic field, magnetic coordinates (*L*, *B/Bo*) are the logical choice for ordering the dose data. The coordinate "L" labels a magnetic field line by the radial distance (in Earth radii) at which it crosses the magnetic equator. The coordinate "B/Bo" is the ratio between the magnetic field *B* at some arbitrary point along a field line and the equatorial (minimum) value *Bo* along that same field line. The CEASE and PASP dose databases are binned and averaged in (*L*, *B/Bo*) in a manner identical to the published APEXRAD model (see [2] and [3] for details). The resulting mission averaged APEX/PASP and TSX5/CEASE dose-rate maps, when displayed on the northern quadrant of a dipolar grid (Fig. 2), aid in visualizing the relevant spatial regions. The inner zone is seen as the darker color contours extending from the equator inside $L = 1.5$, while the outer zone "horns" are seen as darker color contours at high latitudes in the region between $L = 3$ to 5. The heart of the outer radiation belt is the equatorial projection of the $L = 3$ to 5 field lines and exhibit much higher dose rates than those at the low altitudes shown in Fig. 2.

Since the APEX and TSX5 orbits are not identical, regions of (*L*, *B/Bo*) space are sampled differently by the two spacecraft. Simply averaging over the entire range of *B/Bo* for a fixed *L* would yield skewed results because of the different temporal coverage in (*L*, *B/Bo*) and the dose dependency on *B/Bo*. To best compare dose variations seen by PASP and CEASE, a subset of the complete (*L*, *B/Bo*) grid is determined that provides ample observations for the study yet also minimizes the spread in *B/Bo* for a fixed *L* bin width (0.1 R_E). The bottom panel of Fig. 3 illustrates the increasing *B/Bo* bin width as a function of *L*. The top panel illustrates the range of altitudes sampled by the respective satellites corresponding to the specified *L* and *B/Bo* range. For $L < 5.5$, the coverage in altitude is quite constant, where the average range for APEX altitudes is 1355 ± 520 km, and for TSX5, 1270 ± 350 km. Fig. 2 illustrates roughly the region of interest as being enclosed between the $L = 3$ to 5 field lines and between the 1000 to 2000 km altitude arcs. In what follows, it should be understood that within the explicit *L* dependence of dose distributions is an implicit dependence in *B/Bo*.

Subsequent to binning the full resolution (5 s) dose data into the (*L*, *B/Bo*) grid prescribed above, the daily averaged dose rates for both data sets are computed as a function of *L*. These daily dose profiles are plotted as epoch surveys in Fig. 4(a) (APEX/PASP) and Fig. 4(b) (TSX5/CEASE), along with the respective magnetic activity index Dst history for each epoch. The

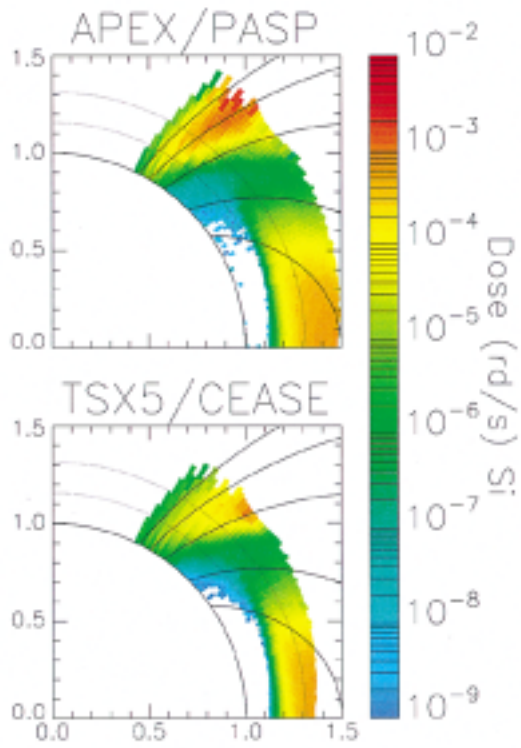

Fig. 2. Mission average dose rates (rd/s) in silicon (color coded) plotted in dipole (*L*, *B/Bo*) coordinates for (top) PASP and (bottom) CEASE. The vertical and horizontal scales are in units of Earth radii. Dipole field lines for $L = 1.5, 2, 3, 4,$ and 5 have been drawn, with the $L = 1.5$ field line shown intersecting the magnetic equator. Dotted circular arcs are drawn at 1000 and 2000 km.

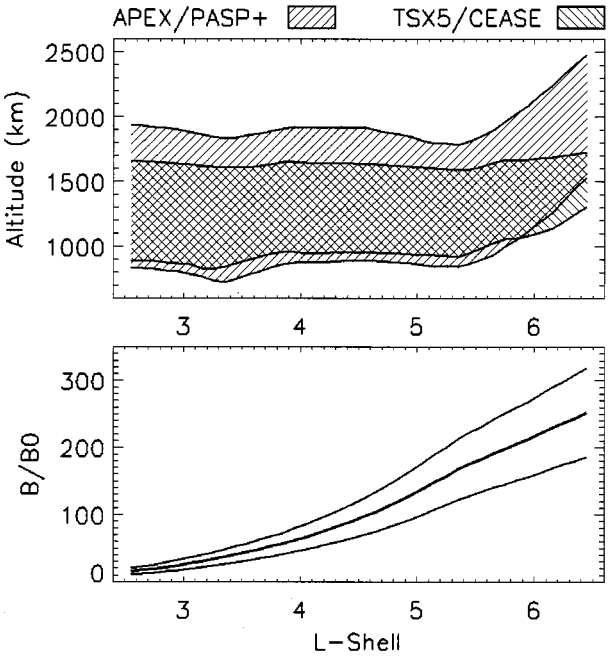

Fig. 3. Dose data are sorted by (*L*, *B/Bo*) coordinates. The *L* bin width is fixed at 0.1 R_E, whereas the *B/Bo* bin width increases with *L*. In the bottom panel, the average *B/Bo* for the two spacecraft is plotted (heavy solid line) versus *L*, with the upper and lower limits of the *B/Bo* bin width defined by ± 0.25 of the average. In the top panel, the altitude coverage for each satellite, defined as $\pm$ one sigma of the average altitude, is plotted versus *L*. The cross-hatched area is where the satellites' coverage overlap.

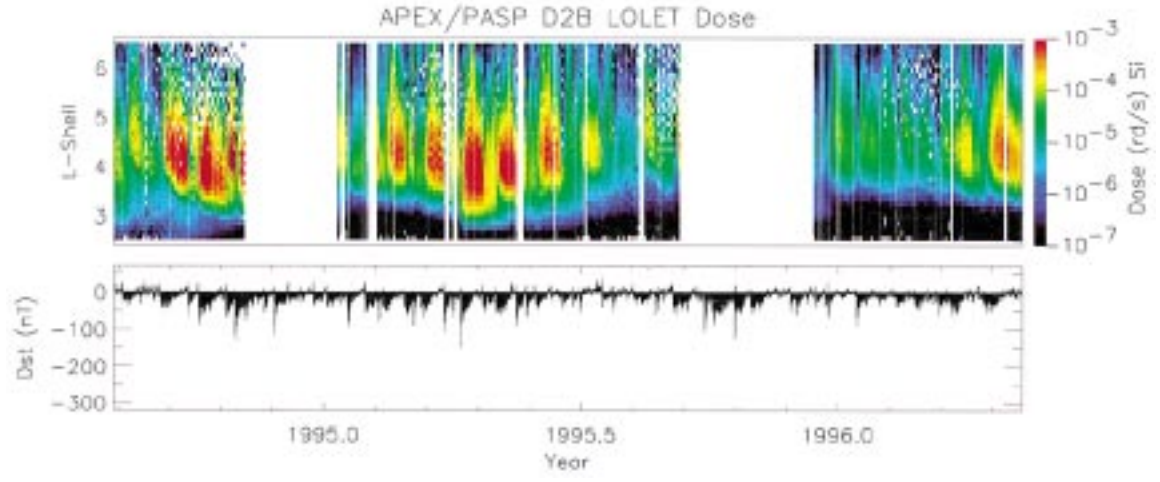

(a)

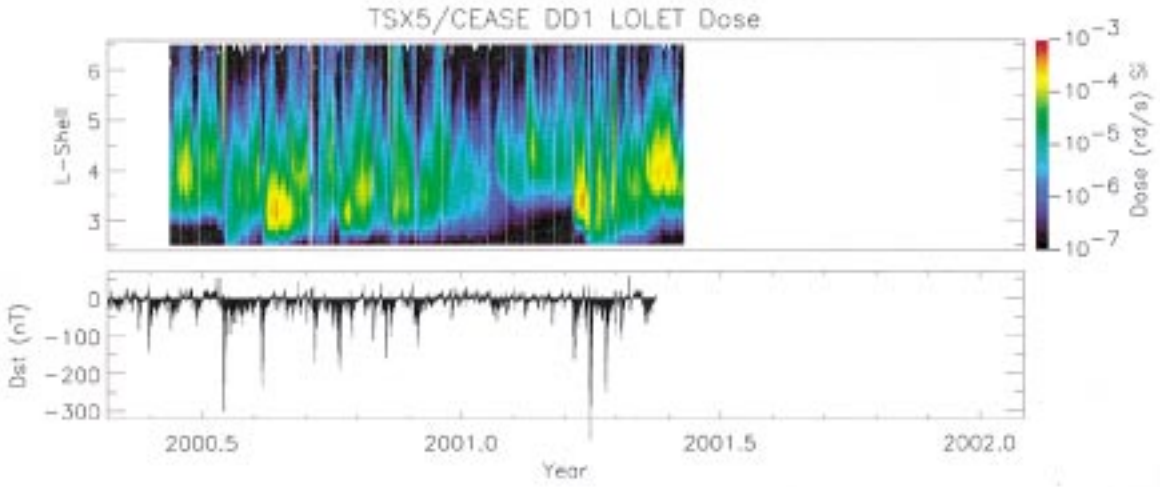

(b)

Fig. 4. Plotted are the (a) APEX and (b) TSX5 mission surveys. The top panel plots does rat (rd/s) in silicon (color coded) as a function of L (implicit *B/Bo* dependence) and year. The bottom panel plots the magnetic activity index Dst (nT) as a function of year. The time scale from both missions are set to be equivalent to facilitate comparison of temporal variations.

PASP dose survey, particularly up through 1995.5, highlights the periodic enhancements of megaelectronvolt electrons characteristically observed during the years approaching solar minimum. Dst is a measure of magnetic storm activity, with a more negative value indicative of greater activity. Periods exhibiting the largest Dst excursions (e.g., during the TSX5 epoch around years 2000.55 and 2001.25) also show the largest increases in dose rates in the slot region (down to $L = 2.5$).

The simplest way to compare the dose rates from the two different epochs is to construct a single average dose model as an explicit function of L from each mission. These average dose profiles are presented in Fig. 5. The average PASP (solar minimum epoch) dose rate is higher and peaks at a higher L value than that for CEASE (solar maximum epoch). The PASP peak dose rate is 1.1×10^{-4} rd/s (at $L = 4.1$), while the CEASE peak dose rate is 3.2×10^{-5} rd/s (at $L = 3.8$). The ratio of PASP to CEASE dose rate decreases from $\sim$5 for $L \sim 4.5$ to $\sim$3 at $L \sim 6.5$. The PASP dose rate peak is also somewhat narrower than the CEASE peak. For comparison, average dose rates at several (L, *B/Bo*) points are computed using spectra from the NASA AE8 models (the AE8 models were downloaded from the Web pages of NASA's National Space Science Data Center). For a given L, the values of *B/Bo* used to specify the AE8MIN (AE8MAX) spectra are the average *B/Bo* from the corresponding APEX (TSX5) ephemeris. The ITS code is used to simulate the transport of the AE8MIN and AE8MAX omnidirectional flux spectra (1 to 7 MeV) through the PASP and CEASE dosimeter models, respectively. These AE8 model predicted dose rates are included in Fig. 5. For $L > 4$, the AE8MAX and AE8MIN models give identical fluxes for a given coordinate pair (L, *B/Bo*). However, due to the slight differences in the average *B/Bo* for the two spacecraft orbits, the AE8MIN and AE8MAX dose predictions for $L > 4$ differ by $\sim$30%, the difference attributed to the variation of spectra with *B/Bo*. For $L \leq 4.5$, the AE8MIN model is less than a factor of two higher than the observed PASP dose. For $L > 4$, the ratio of AE8MIN to PASP increases steadily to $\sim$5 near geosynchronous. The agreement between AE8MAX and CEASE is much less, with the ratio of AE8MAX to CEASE increasingly steadily from $\sim$6 at $L = 3.5$ to $\sim$10 near geosynchronous.

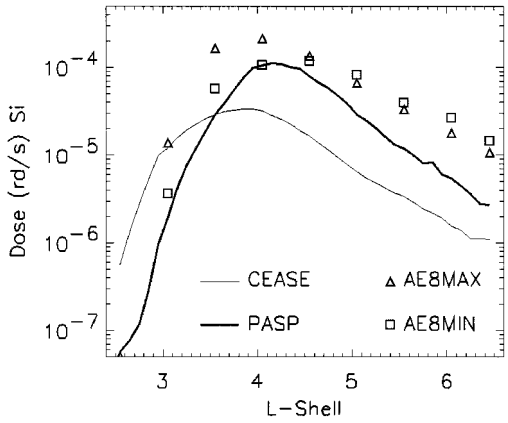

Fig. 5. APEX/PASP (heavy line) and TSX5/CEASE (thin line) mission average dose rates (rd/s) in silicon as a function of L (implicit B/Bo dependence). Predicted dose rates from AE8MIN (squares) and AE8MAX (triangles) are included for comparison.

In addition to long-term average dose models, which obscure the wide dynamic variations of the outer belt electrons, space system design engineers are interested in the probability of exceeding a given dose rate at a fixed point in space. To construct these distributions, the observed dynamic range of dose rates (spanning five orders of magnitude, 10^{-7} to 10^{-2} rd/s) is divided into 50 equal logarithmically spaced bins. For each L bin, the fraction of 5-s dose measurements falling within each dose rate bin is determined such that the integral over all dose rate bins sums to one. The probability for exceeding a given dose rate D is then determined by integrating over these dose rate bins from D to D_{max} (10^{-2} rd/s). These probability distributions, for both APEX and TSX5 missions, for all L, are shown in Fig. 6(a) and (b). The shape of the dose profiles (in L) seen in Fig. 5 is reflected in Fig. 6. To facilitate a direct comparison of the probability distributions for the two epochs, the distributions at a single L near the dose peak ($L = 4$) are plotted together in Fig. 7. From this plot, it can be seen that for these missions, the probability of exceeding the dose rate of 10^{-4} rd/s is $\sim$0.38 during the solar minimum epoch (APEX) and $\sim$0.10 during the solar maximum epoch (TSX5). It should be emphasized that these probabilities have been derived from a specific range of (L, B/Bo) space. For the case here of $L = 4$, B/Bo ranges between 48 and 80 and is not representative of the dose environment for $L = 4$ on the equator ($B/Bo = 1$) where dose rates are considerably larger.

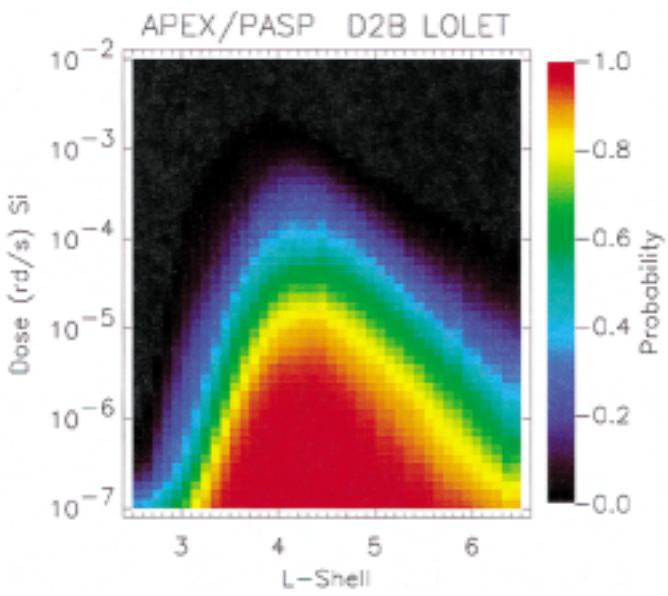

(a)

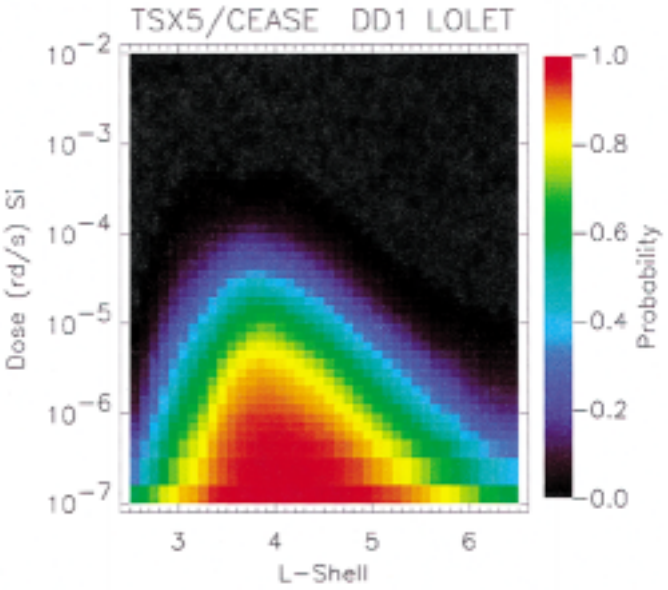

(b)

Fig. 6. (a) PASP (solar minimum epoch) and (b) CEASE (solar minimum epoch) probabilistic dose models give probability (color coded) for exceeding specified dose rat (rd/s in silicon) plotted as a function of dose rate and L.

IV. Discussion

One clear result here is that for $L > 4$, the mission averaged PASP (solar minimum epoch) dose rates are a factor of $\sim$4 higher than those for CEASE (solar maximum epoch), a significant departure from the nearly equal rates predicted by the NASA AE8 models. This result is consistent with recent studies, which attribute periodic enhancements of megaelectronvolt electron flux at geosynchronous to the HSSWS prominent during the approach toward solar minimum [7]–[9]. This 27-day periodicity in enhancements of megaelectronvolt electrons is evident in the PASP dose seen in Fig. 4(a), where the enhanced dose rates are observed throughout a wide range of L spanning the "horns" of the outer radiation belt.

A second result is that the average dose profile for CEASE (solar maximum epoch) peaks at a lower L ($L = 3.8$) and has a broader peak than does the dose profile for PASP (solar maximum epoch), which peaks at $L = 4.1$. This result is attributed to the greater number of magnetic storms occurring during solar maximum. The difference in geomagnetic activity for the two epochs is apparent in the plots of Dst in Fig. 4, where maximum negative excursion in Dst corresponds to the severest magnetic storm activity. Although there were comparable numbers ($\sim$6) of moderate storms (Dst $= -100$ to -150 nT) during both epochs, there were eight major storms (Dst < -150 nT) during

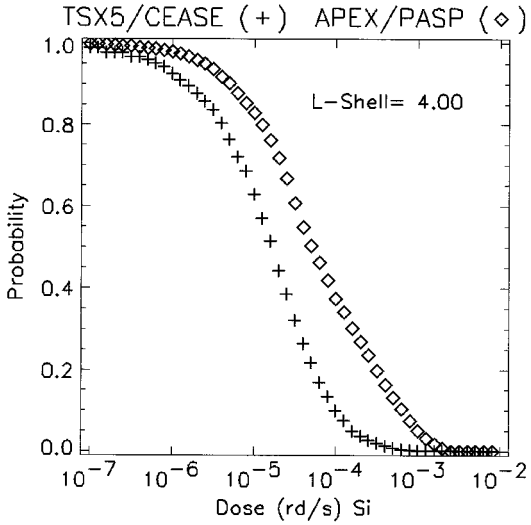

Fig. 7. This plot is a two-dimensional representation of the information in Fig. 6(a) and (b) for $L = 4.0$. It gives the probability that the PASP (triangle) and CEASE (cross) dose rate at $L = 4$ exceeds some specified threshold level (independent variable).

the TSX5 epoch, with none during the APEX epoch. Associated with these largest storms are the injections of dose producing electrons that penetrate deep into the slot region ($L \sim 2.5$). The greater frequency of these storms during solar maximum moves the inner edge of the average dose profile to lower L and broadens the profile peak.

Future work will investigate the possibility of extending the spatial coverage of *in situ* dose measurements by developing algorithms for mapping dose along field lines to other remote regions and by interpolating between other existing spacecraft. Although this study dealt with the LoLET dose behind 80 mil of Al corresponding to >1 MeV electrons, future work will analyze a second CEASE channel for dose behind 250 mil of Al corresponding to >3 MeV electrons. The relative dose from these two channels may then be used to examine the spatial–temporal variability of spectral hardness of this very dynamic trapped particle population.

V. Summary

The significance of the outer zone electrons, in terms of both their effect on space technologies [4], [5] and human safety [4], [6], is well known. However, much work is required to better characterize this population's variability over solar cycle time scales. Whereas long-term averages were once the model standard, it is becoming increasingly evident that more detailed information on the extremes and the variability of the environment is advantageous for both satellite design engineers and those responsible for planning human activities in space.

This study has produced results that are consistent with studies utilizing geosynchronous flux data, which found that electron enhancements minimize near solar maximum and maximize during the approach to solar minimum. The discrepancy with the NASA AE8 models underscores the need to promote further improvement of existing radiation models by continually monitoring the radiation belts throughout the solar cycle. This study has also produced some probabilistic models as a step toward an alternative to the standard mission averaged model. Although the study's spatial coverage is limited to low Earth orbit, and its temporal coverage to <3 years of an 11-year solar cycle, it does provide a framework for incorporating future data sets. More CEASE units are scheduled to fly in the future, and these data will continue to expand the current spatial-temporal coverage leading to improved modeling capabilities.

Acknowledgment

D. H. Brautigam would like to thank E. G. Mullen and M. S. Gussenhoven for valuable discussions and for laying the groundwork for this study over their many years at AFRL.

References

[1] B. K. Dichter, J. O. McGarity, M. R. Oberhardt, V. T. Jordanov, D. J. Sperry, A. C. Huber, J. A. Pantazis, E. G. Mullen, G. Ginet, and M. S. Gussenhoven, "Compact Environmental Anomaly Sensor (CEASE): A novel spacecraft instrument for *in situ* measurements of environmental conditions," *IEEE Trans. Nucl. Sci.*, vol. 45, no. 6, pp. 2758–2764, 1998.

[2] M. S. Gussenhoven, E. G. Mullen, D. A. Hardy, D. Madden, E. Holeman, D. Delorey, and F. Hanser, "Low altitude edge of the inner radiation belt: Dose models from the APEX satellite," *IEEE Trans. Nucl. Sci.*, vol. 42, no. 6, pp. 2035–2042, 1995.

[3] M. S. Gussenhoven, E. G. Mullen, J. T. Bell, D. Madden, and E. Holeman, "APEXRAD: Low altitude orbit dose as a function of inclination, magnetic activity and solar cycle," *IEEE Trans. Nucl. Sci.*, vol. 44, no. 6, pp. 2161–2168, 1997.

[4] J. Feynman and S. B. Gabriel, "On space weather consequences and predictions," *J. Geophys. Res.*, vol. 105, pp. 10 543–10 564, 2000.

[5] A. R. Frederickson, "Upsets related to spacecraft charging," *IEEE Trans. Nucl. Sci.*, vol. 43, no. 6, pp. 426–441, 1996.

[6] Space Studies Board, National Research Council, Radiation and the International Space Station, *Recommendations to Reduce Risk*: National Academy Press, 2000.

[7] D. N. Baker, J. B. Blake, R. W. Klebesadel, and P. R. Higbie, "Highly relativistic electrons in the Earth's outer magnetosphere: 1. Lifetimes and temporal history 1979–1984," *J. Geophys. Res.*, vol. 91, pp. 4265–4276, 1986.

[8] G. L. Wren, D. J. Rodgers, and P. Buehler, "Modeling the outer belt enhancements of penetrating electrons," *J. Spacecraft Rockets*, vol. 37, pp. 408–415, 2000.

[9] D. N. Baker, R. A. Goldberg, F. A. Herrero, J. B. Blake, and L. B. Callis, "Satellite and rocket studies of relativistic electrons and their influence on the middle atmosphere," *J. Spacecraft Rockets*, vol. 55, no. 13, pp. 1619–1628, 1993.

[10] M. S. Gussenhoven, E. G. Mullen, R. C. Filz, and D. H. Brautigam, "New low altitude orbit measurements," *IEEE Trans. Nucl. Sci.*, vol. NS-34, no. 6, pp. 676–683, 1987.

[11] M. S. Gussenhoven, E. G. Mullen, D. H. Brautigam, and E. Holeman, "Dose variation during solar minimum," *IEEE Trans. Nucl. Sci.*, vol. 39, pp. 1671–1677, 1991.

[12] M. S. Gussenhoven, E. G. Mullen, and E. Holeman, "Radiation belt dynamics during solar minimum," *IEEE Trans. Nucl. Sci.*, vol. 36, pp. 2008–2014, 1989.

[13] J. D. Gaffey, Jr. and D. Bilitza, "NASA/National space science data center trapped radiation models," *J. Spacecraft Rockets*, vol. 31, pp. 172–176, 1994.

[14] K. J. Kerns and M. S. Gussenhoven, "CRRESRAD documentation," Phillips Laboratory, AFMC, Hanscom, AFB, MA, PL-TR-92-2201, 1992.

[15] D. H. Brautigam, M. S. Gussenhoven, and E. G. Mullen, "Quasistatic model of outer zone electrons," *IEEE Trans. Nucl. Sci.*, vol. 39, no. 6, pp. 1797–1803, 1992.

[16] E. J. Daly, J. Lemaire, D. Heynderickx, and D. J. Rodgers, "Problems with models of the radiation belts," *IEEE Trans. Nucl. Sci.*, vol. 43, no. 2, pp. 403–415, 1996.

[17] M. S. Gussenhoven, E. G. Mullen, and D. H. Brautigam, "Near-earth radiation model deficiencies as seen on CRRES," *Adv. Space Res.*, vol. 14, no. 10, pp. 927–941, 1994.

[18] J. A. Halbleib *et al.*, "ITS—Integrated TIGER Series of coupled electron/photon Monte Carlo code system," ORNL RSICC Computer Code Package CCC-467.